

Nanoscale Structure and Compositional Analysis of Manganese Oxide Coatings on the Smithsonian Castle, Washington, DC

Meredith C. Sharps^{†‡}, Carol A. Grissom[‡], and Edward P. Vicenzi^{†*}

[†]Department of Chemistry and Biochemistry, University of Oregon, Eugene, Oregon 97403, United States

[‡]Smithsonian Institution, Museum Conservation Institute, 4210 Silver Hill Road, Suitland, MD 20746, United States

*Corresponding author: vicenzie@si.edu

Abstract

The Smithsonian Castle is a historic building in Washington, D.C. that was erected almost 165 years ago and served as the first home for the Smithsonian Institution. Currently, the building exhibits dark surface discoloration due to manganese-rich coatings that are growing in patches across its Seneca sandstone exterior. Bulk and microanalysis of this coating indicate that it is consistent with rock varnish, but the coating is difficult to analyze without contribution from the underlying minerals that comprise the sandstone. To address this limitation, SEM/FIB-prepared cross-sections of the coating were analyzed using HRTEM, STEM-EDX, and SAED analyses in order to study the nanoscale structure and composition of the Mn-rich coating in isolation, without convolution from the sandstone. Structurally, the coating is <1 μm thick, polycrystalline, and composed primarily of birnessite, a layered manganese oxide. High spatial resolution data reveal that the coating is Ca-bearing, with only minor quantities of Fe, Si, and Al, distinguishing it compositionally from typical manganese rock varnish and classifying it instead as a manganese skin. TEM revealed layers of aeolian detritus below and a thin silica glaze above the Mn-rich coating, providing a relative timeline of formation. Nanoscale particulates of barite found within the Mn-rich coating, along with the micro- and nanoscale detritus below the coating, indicate atmospheric deposition as the main source for both Mn and Ba. The compositional and structural

information gathered from these analyses helps constrain mechanisms of formation towards a biological origin; however, no direct evidence for Mn oxide producing microorganisms was observed.

Keywords

Rock varnish, manganese oxide, metal skin, birnessite, microanalysis, microstructure

1 Introduction

The Smithsonian Institution Building, commonly known as the “Castle”, was completed in 1855 as the first home for the Smithsonian Institution in Washington, D.C. The Castle originally served as the residence for the Smithsonian’s first secretary, physicist Joseph Henry, and also housed exhibits, laboratories, and lecture halls (Peck, 2013). The building was designed by James Renwick Jr. in a Romanesque style and is clad with Upper Triassic red Seneca sandstone, an arkosic micaceous sandstone originating from the Bull Run Quarry in Seneca, MD. Recently, Seneca sandstone was designated as a Global Heritage Stone Resource owing to its significance and prominence in early American architecture (Grissom et al., 2018).

In 2007, discoloration in the form of dark bluish-black patches was observed on all façades of the Castle. Portable X-ray fluorescence (XRF) measurements revealed these patches contain elevated levels of manganese relative to the bulk sandstone (Grissom et al., 2014), a feature consistent with rock varnish. Rock varnish is composed of clay minerals intimately mixed with manganese and iron oxides, and it adheres to host rock as a dark crust. It accumulates slowly and is considered the slowest growing sedimentary deposit: growth rates are estimated between 1-40 $\mu\text{m}/\text{ka}$ on subaerial rock surfaces (Liu and Broecker, 2000; Macholdt et al., 2018). The slow growth and accumulation of varnish has made it of interest in fields such as anthropology (Dorn et al., 2012b; Elvidge and Moore, 2013), paleoclimate and paleoenvironment (Broecker and Liu,

2001), geologic or anthropological dating (Liu and Broecker, 2007; Liu and Broecker, 2008; Macholdt et al., 2019), and astrobiology (Allen et al., 2004; Krinsley et al., 2009). Despite being studied for over 200 years (Humboldt and Wilson, 1995) and in a variety of fields, the mechanisms of manganese enrichment and transport are still incompletely understood.

Clay minerals are the dominant component of rock varnish, comprising about 70% of the composition (Potter and Rossman, 1977). These minerals likely arrive at rock surfaces via atmospheric transport (Dorn, 2007; Dorn et al., 2013; Fleisher et al., 1999; Perry and Adams, 1978) and are then slowly cemented to the surface through manganese and iron oxide formation. It has long been debated how manganese enrichment occurs in the varnish, as it is normally found in a >50x concentration over manganese in the underlying rock or soil. The manganese phases in varnish are predominantly layered or tunneled oxide structures related to birnessite and todorokite phases of Mn minerals but are typically poorly crystalline (McKeown and Post, 2001). Three main hypotheses exist to explain manganese enrichment in varnish genesis: 1) enrichment occurs abiotically through local physicochemical changes at the surface of the host rock, oxidizing Mn^{2+} to Mn^{4+} (Engel and Sharp, 1958; Thiagarajan and Aeolus Lee, 2004); 2) enrichment occurs through biological mediation, where microbes produce birnessite-family minerals at the surface of the stone (Nealson, 2006; Northup et al., 2010; Tebo et al., 2004); or 3) a polygenetic model, combining aspects of both the abiotic and biotic hypotheses (Dorn, 2007; Krinsley, 1998).

Rock varnish is found most prominently on rock surfaces in arid environments, where it is called 'desert varnish', and it has been extensively studied in these climates (Dorn, 2007; Engel and Sharp, 1958; Fleisher et al., 1999; Garvie et al., 2008; Liu and Broecker, 2007; Perry and Adams, 1978; Potter and Rossman, 1977; Thiagarajan and Aeolus Lee, 2004). However, rock varnish is ubiquitous and can be found in a variety of climates and locations worldwide, including

tropical and polar environments (Dorn and Krinsley, 2011; Dorn et al., 1992; Macholdt et al., 2017b). Varnish is less well studied in wetter environments, and the presence of varnish on the Castle is one of few documented examples of this surface coating forming on a historic stone surface with a known age (Casanova Municchia et al., 2016; Macholdt et al., 2017a; Vicenzi et al., 2016).

Examining the Smithsonian Castle's varnish offers a rare opportunity to study incipient varnish formation. The Castle's age (~165 years) means that this varnish is both young and rapidly forming relative to those formed over 1-100s ka in geological settings. Previous microanalytical studies on the Castle and on the Enid A. Haupt Garden gateposts (composed of Seneca sandstone and erected adjacent to the Castle in 1987) revealed that the varnish is poorly crystalline, contains elevated levels of lead, lacks microstratigraphy, and is deposited in two different forms: as a discontinuous nanoscale thin film on the surface and as nanoparticles embedded along grain boundaries, extending up to 250 μm into the sandstone (Livingston et al., 2016; Macholdt et al., 2017b; Vicenzi et al., 2016). However, quantification of the Mn-rich layer by surface microanalysis alone is complicated by variabilities in surface roughness, thickness, and the non-uniform coverage of the varnish.

In this study, we inform the structure and composition of the Mn-rich coating on the Smithsonian Castle using a variety of TEM-based techniques, including high resolution (HR) TEM, selected area electron diffraction (SAED) and scanning transmission electron microscopy-based energy dispersive X-ray spectroscopy (STEM-EDX). This nanoscale analysis reveals new information about the thickness, composition, and structure of the Mn-rich layer that is not evident from surface microanalysis alone. The high spatial fidelity of these techniques allows us to observe fine-scale features like the nano-stratigraphy, nanoscale inclusions within the Mn oxide, layers of

atmospherically derived particulates, and a nanoscale thin film of silica glaze, all of which offer insight into a possible timeline of formation. Finally, we discuss the compositional and structural results in the context of other Mn-rich coatings found in similar environments.

2 Materials and Methods

We analyzed a sample from the west-facing façade of the Smithsonian Castle that was well-covered with varnish (Figure 1a). The surface of the sandstone is rough, with areas ranging in height up to ~1 mm. Images of the sample were first acquired with a HIROX digital optical microscope prior to being carbon coated and imaged using a Hitachi S3700N SEM (Figure 1b,c). Hyperspectral X-ray imaging of the film was used to manually select areas enriched in Mn. Derived spectra from these fields-of-view were summed and quantified. Reconstructions of segmented backscattered electron (BSE) images were processed with Digital Surf MountainsMap® software to create a digital elevation map (Figure 1d). These height maps were used to locate areas that were relatively flat (~10s of microns) compared to the height differences within the entire sample (~1 mm) and had good coverage of rock varnish for subsequent FIB cross-section preparation.

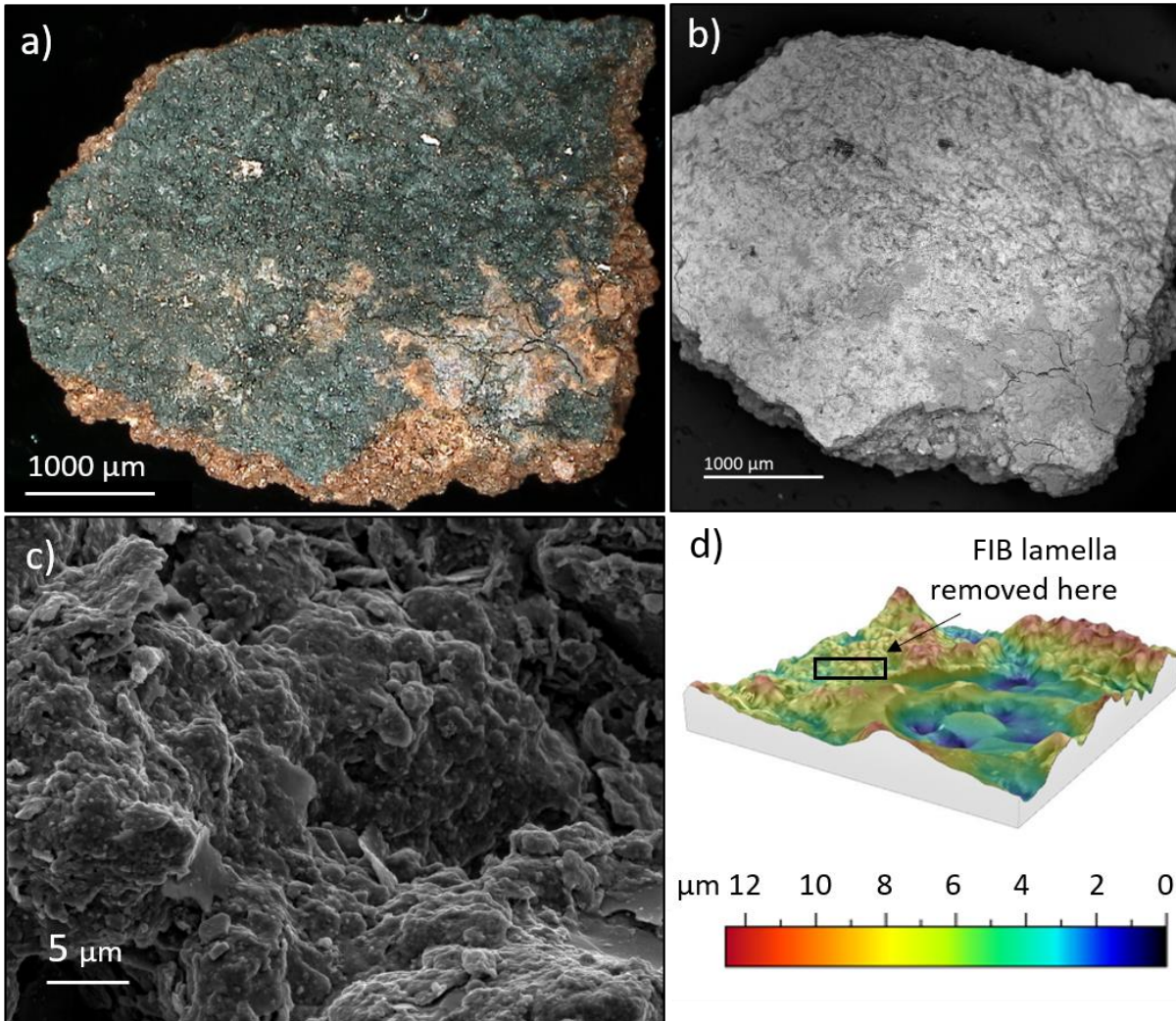


Figure 1: a) Visible light microscope image of the sample analyzed. The dark surface coating can be seen in contrast to the red Seneca sandstone underneath. b) BSE image of the same surface shown in (a). Areas lighter in contrast correspond to higher average atomic number compositions, and in this case those intensities represent Mn-rich zones. c) SE image showing the rough surface topography. d) Three-dimensional topographic map from which a FIB lamella was removed. Areas in red correspond to the highest elevations, while areas in blue-black correspond to the lowest elevations.

In order to find areas thickly covered with varnish, we measured compositions within the digitally height mapped areas using a 10 mm² Bruker XFlash 4010 silicon drift detector (SDD) at accelerating voltages ranging from 5 to 20 kV. Because the Mn is concentrated at the surface, we determined at what voltage the Mn signal was overwhelmed by elemental signatures from the sandstone substrate. Data were simulated in DTSA-II software (Ritchie, 2009), modeling the

varnish on sandstone as a thin film of MnO_2 with a theoretical density of 3 g/cm^3 on an SiO_2 substrate. Using this method, we estimated varnish layer thickness to be from 1.7-2.3 μm and chose areas for FIB removal that were in this range.

Ultrathin cross-sections were prepared on the previously identified areas using an FEI Helios Nanolab 600i FIB-SEM. As the lamellae approached electron transparency, low energy milling was used to mitigate excessive gallium implantation and to avoid damaging any crystallinity in the sample. The prepared samples were imaged in transmission using an FEI Titan 80-300 S/TEM in high angle annular dark-field (HAADF) STEM mode and in bright-field (BF) mode at 300 kV. Each cross-section was then examined using STEM-EDX analysis to probe composition, SAED to determine crystallinity, and HRTEM to observe fine scale structure. These measurements were taken at the Center for Advanced Materials Characterization in Oregon (CAMCOR), located at the University of Oregon.

We performed micro-X-ray fluorescence ($\mu\text{-XRF}$) on a Bruker M4 Tornado equipped with a Rh source, a 20 μm X-ray optic (at $\text{Mo K}\alpha$), a 100 μm aluminum filter, and two XFlash 6|60 SD detectors to analyze the bulk composition of Seneca sandstone sourced from the Bull Run Quarry in Seneca, MD. The sandstone sample was mounted in epoxy and cut to reveal an area of 19.8 mm x 12.7 mm (Figure S1). The sample was mapped at 50 kV with a source current of 550 μA and was scanned at 10 ms/pixel.

3 Results and Discussion

3.1 Nanoscale structure and crystal phase determination

Four FIB cross-sections were taken from a sample of the Smithsonian Castle sandstone in an area where patches are darkly coated in varnish, shown in Figure 1a. The varnish layer is clearly visible upon first imaging the FIB cross-sections by SEM (Figure 2a). Our original estimation of

layer thickness based on plan-view EDS and stochastic modeling with DTSA-II software was between 1.7 and 2.6 μm . The FIB cross-sections of these areas, however, showed that across all four FIB lamellae, the film is $<1\mu\text{m}$ thick, ranging from $\sim 150\text{ nm}$ at its thinnest to $\sim 900\text{ nm}$ at its thickest. The difference between our estimation and experimental measurements likely arises from assumptions regarding composition, density, and heterogeneity used in thin film modeling. The model approximates the material with a thin, flat film of MnO_2 on a flat SiO_2 substrate. In reality, the Mn-rich film conforms to the topography of the sandstone surface, which ranges in height in the areas examined by 10s of microns. Previous studies have shown that the varnish also extends into the sandstone grain boundaries up to $250\mu\text{m}$ (Vicenzi et al., 2016). Any additional Mn signal from this area beneath the surface layer would inflate the modeled thickness estimate. Although all of our FIB cross-sections had thicknesses $<1\mu\text{m}$, it is important to note that the FIB lamella taken by Macholdt et al. (2017b) was extracted from the same specimen and shows a varnish layer of $\sim 4\mu\text{m}$, revealing a large thickness range across a spatial area of a few centimeters. Large variations in the thickness of Mn-rich coatings have also been reported elsewhere for both wet climates (Casanova Municchia et al., 2016; Dorn et al., 2012a) and for rapidly forming varnishes (Spilde et al., 2013).

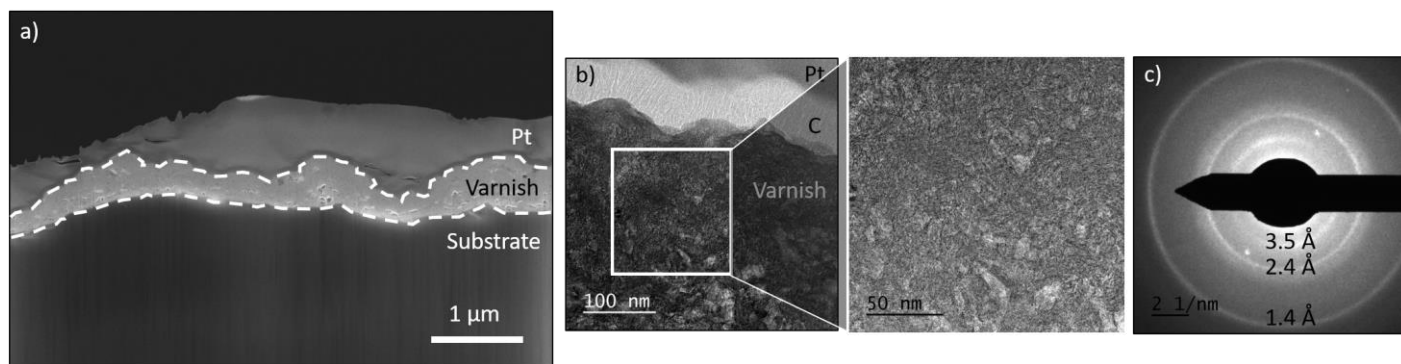


Figure 2: a) Secondary electron image of a FIB cross-section of the varnish layer. A thin layer of electron beam deposited carbon and a layer of ion beam deposited platinum were applied to the top surface. b) Bright-field TEM image of the top area of the varnish. The inset shows the area

that was taken for the corresponding diffraction pattern. c) The three rings in the SAED pattern indexed to birnessite.

Rock varnish and naturally formed manganese oxides in general are poorly crystalline and difficult to observe via bulk X-ray diffraction (Post, 1999). We used SAED to determine whether the Castle varnish was crystalline on the nanoscale and investigated consistency of the phase by looking at twenty-seven different areas across all four FIB lamellae. At each area (example Fig. 2b), we observed a consistent, diffuse, three-ring pattern (Figure 2c), indicating that the varnish layer is polycrystalline on the nanoscale. These SAED patterns were indexed to average lattice spacings of 1.4, 2.4, and 3.5 Å, consistent with birnessite, $(\text{Na,Ca})_{0.5}(\text{Mn}^{4+}, \text{Mn}^{3+})_2\text{O}_4 \cdot 1.5 \text{H}_2\text{O}$ (Anthony et al., 1997). Imaging the varnish with HRTEM (Figure 3 a,b) showed clear and defined layers with an average 7.2 Å spacing. This inter-layer distance is also consistent with the sheet-like structure of birnessite, shown in the example crystal structure in Figure 3c. We did not observe lattice spacing or tunneling structures indicative of todorokite, the other most common phase reported in the rock varnish literature. The consistency of the diffraction patterns and the layered spacing indicate that birnessite is relatively pure across the four lamellae analyzed.

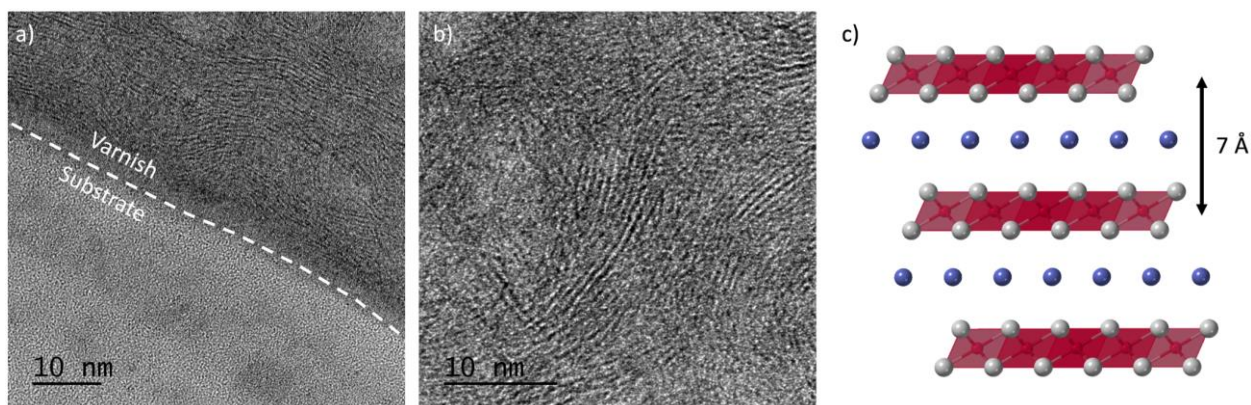


Figure 3: High resolution TEM images. a) The interface where the varnish layer meets the substrate, in this case a grain of quartz. b) A higher magnification image of the layering in the varnish layer alone shows the visible layers that are spaced an average of 7.2 Å apart. c) Structure of birnessite, showing Mn sheets spaced 7 Å apart with cations in the interlayer spacing. Mn (red), O (grey), interstitial cation (blue). The actual distance between the layers varies slightly depending on the cations in the interstitial space. Adapted from the crystal structure of synthetic birnessite by Lanson et al. (2002).

3.2 Elemental distribution, nanoscale inclusions, and atmospheric deposition

We analyzed the composition of the varnish using STEM-EDX of the FIB cross-sections. The varnish layer is composed of a large fraction of Mn, with only about one atomic percentage coming from Fe, Si, and Al each (Table 1). This was an unexpected result, as we anticipated a higher percentage of clay minerals based on other representative varnish samples found throughout the literature (Dorn, 2007). A comparison of weight percentages between the data found here and other microanalyses of Mn-rich coatings can be found in Table S1 in the supporting information. Elemental mapping revealed that the most abundant element in the Mn-rich layer besides Mn and O is Ca (Figure 4), suggesting that the major phase of the varnish is a Ca-rich birnessite. This Ca enrichment is consistent with observed correlations by Raymond et al. (1992) and common among many different classes of varnish as confirmed by Macholdt et al. (2017b). Calcium typically resides as an adsorbed species between the layered Mn oxide sheets (Drits et al., 1998; Post, 1999). Although Ca is the most abundant interlayer element observed throughout the varnish, we also found a variety of minor elements distributed nearly uniformly, including Si, Al, P, S, Fe, Mg, Na, Ba, K, Pb, and Zn. These elements are likely adsorbed at interlayer sites, at Mn octahedral vacancies, or at external edge sites in the crystal structure (Tebo et al., 2004; Villalobos et al., 2005; Wang et al., 2012). By normalizing the Mn atomic concentration to 2, we estimate a stoichiometry of $\text{Ca}_{0.3}\text{Mn}_2\text{O}_{4.4}$, with the remaining minor cations having stoichiometric values < 0.1.

Table 1: STEM-EDX analyses for the Mn-rich layer. Values are reported as atomic percentages.

Element	O	Mn	Ca	Fe	Si	Al	Ba	Pb	S	P	K	Zn	Mg	Na
Site 1a	59.79	29.25	4.90	1.64	0.28	0.96	0.26	0.19	0.34	1.38	0.47	--	0.53	--
Site 1b	60.55	27.94	4.64	1.08	1.11	1.08	0.30	0.20	0.62	1.13	0.45	0.13	0.56	0.07
Site 1c	54.36	27.85	3.86	1.85	0.64	0.62	0.32	0.19	0.30	1.10	0.44	0.15	0.36	0.09
Site 2a	59.87	27.47	4.92	0.57	1.25	1.18	0.71	0.16	1.47	1.39	0.32	0.16	0.35	0.11
Site 2b	59.80	27.30	4.95	0.68	1.93	1.21	0.51	0.13	1.26	1.23	0.27	0.17	0.37	0.12
Site 2c	60.12	27.27	4.96	0.66	1.69	1.28	0.31	0.15	1.08	1.38	0.29	0.17	0.46	0.12
Site 2d	58.05	28.52	5.04	0.73	2.17	1.29	0.45	0.14	1.12	1.42	0.29	0.22	0.47	0.10
Site 3a	62.43	27.09	3.92	0.53	0.54	1.22	0.37	0.10	0.67	1.30	0.32	0.20	0.68	0.47
Site 3b	58.65	28.47	3.67	0.71	0.96	1.23	0.43	0.10	0.33	1.20	0.36	0.17	0.49	3.06
Site 3c	62.34	26.32	4.07	0.59	0.95	1.42	0.55	0.08	0.83	1.27	0.34	0.17	0.59	0.24
Site 4a	61.94	25.91	5.12	0.75	1.23	1.39	0.28	--	0.74	1.40	0.37	0.17	0.53	--
Site 4b	61.32	26.77	5.24	0.64	0.74	1.41	0.22	0.09	1.05	1.34	0.39	0.19	0.48	0.13
Average	59.94	27.51	4.61	0.86	1.12	1.19	0.39	0.14	0.82	1.30	0.36	0.17	0.49	0.45
St. Dev.	2.23	0.95	0.56	0.43	0.57	0.22	0.14	0.04	0.39	0.11	0.07	0.03	0.10	0.92

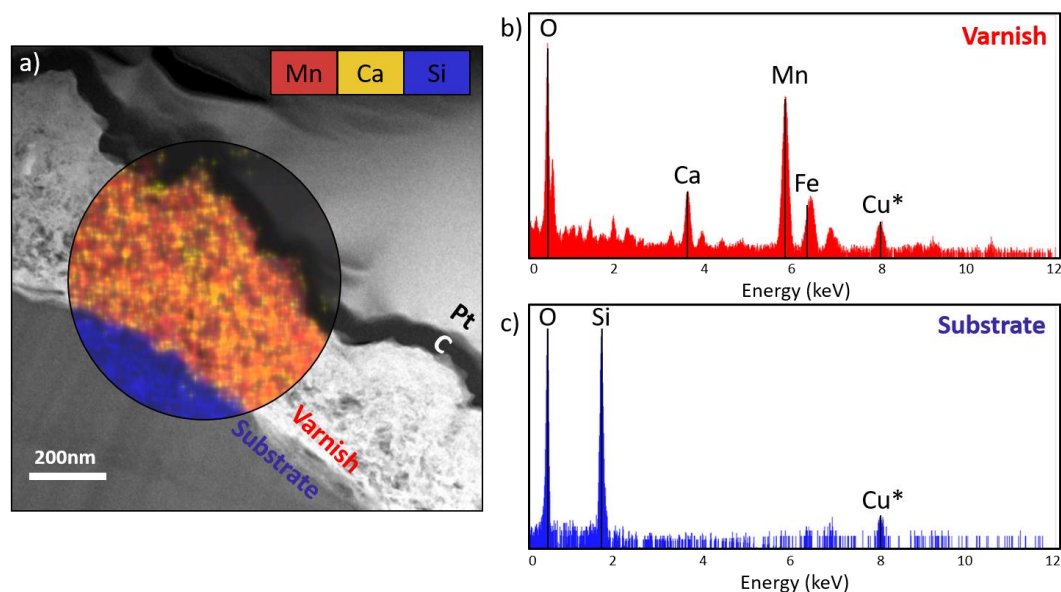


Figure 4: a) HAADF STEM image of a FIB cross section. The colored circle represents areas that were mapped using EDX. b-c) Corresponding X-ray spectra are shown for the varnish and substrate layers with only the major peaks labeled. Atomic percentages for minor elements found uniformly throughout the varnish layer are shown in Table 1. *The Cu peak arises from the copper TEM grid.

In addition to the various minor elements found in the varnish layer, STEM-EDX mapping also revealed that separate, nanoscale particulates (~50-100 nm) are also incorporated into the Mn-coating. Stoichiometries from the EDX measurements and associated SAED patterns of some of

the particulates helped us to identify clays, plagioclase feldspars, quartz, hematite, gypsum, and barite in the coating (Figure 5). Many of these same minerals found as particulates in the varnish layer are also present in considerable quantities in the Seneca sandstone, except for gypsum and barite. A μ XRF map taken across a sample of sandstone from the Bull Run Quarry shows that Ba is present at a level of ≈ 49 ppm (Figure S1). In contrast, it is $>300x$ that concentration in the Mn-rich surface layer.

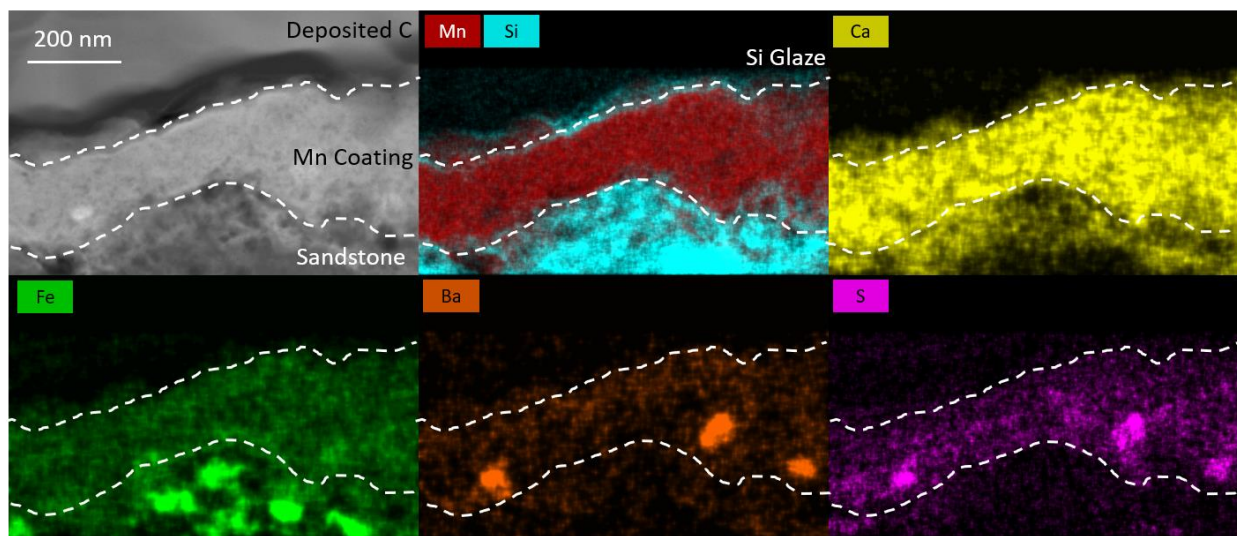


Figure 5: HAADF STEM image of the Mn-rich coating is shown in the top left. Single or dual element EDX maps of the same area show the locations where each element is concentrated. Dashed lines are drawn to guide the eye to the boundaries of the Mn-rich layer. Fe-rich particles lie just below the Mn coating, while particulates rich in Ba and S, indicative of barite, are found within the coating. Finally, Si is present not only in the sandstone below the Mn coating, but also above it, suggesting the formation of an ultrathin silica glaze.

Barium is often present in rock varnishes to a varying degree depending upon type of varnish and location where it is found (Macholdt et al., 2017b). Cationic Ba^{2+} typically resides in interlayer or inter-tunnel sites in Mn oxides (such as in hollandite and romanechite) owing to its large atomic radius (Post, 1999). Ba^{2+} is thought to stabilize tunneled structures associated with todorokite (Tebo et al., 2004). In other studies, barite has been observed in varnish, but these coincide with other structural changes, such as Mn rimmed pores or mineral coarsening, that

indicate diagenesis: the dissolution of Ba-bearing Mn oxides and subsequent precipitation of barite as a secondary mineral (Garvie et al., 2008; Reneau et al., 1992). In our study, we only observe the sheet structure associated with birnessite family minerals, so it is unlikely that Ba²⁺ is impacting the structure and phase of the varnish at this point in its development. There is also no other structural evidence indicating diagenesis as a plausible method of barite formation, and the paucity of Ba in the Seneca sandstone relative to the Mn-rich layer makes the sandstone an unlikely source for the element. Instead, accumulated dust at the sandstone surface provides evidence for atmospheric deposition of barite.

Of the four extracted FIB lamellae, two samples contain varnish films directly on quartz or feldspar grains of the sandstone while the other two samples have fine-scale particles sandwiched between the sandstone and the varnish (Figure 6). STEM-EDX analysis of the detritus revealed nano- and microscale particles of quartz, feldspar, hematite, gypsum, phyllosilicates, and barite – the same types of particulates observed within the varnish itself (Figure S2). The presence of barite in this particulate layer indicates that the particles arrived through atmospheric deposition prior to varnish formation. Atmospheric deposition of barite is also supported by a recent analysis of ~40,000 dust particles collected near the Castle, which identified and categorized various classes of compounds based upon composition (Ortiz-Montalvo et al., 2018). From these analyses, a likely source of Ba emerged within one of the “vehicle-related” classes of particles (Ortiz-Montalvo et al., 2018). Vehicle emissions have also been identified as a source for Ba found in Mn-crusts on the Freiburger Münster in Germany (Macholdt et al., 2017a). BaSO₄ is commonly found as a filler in brake pads of automobiles (Lu et al., 2002) and can be released into the atmosphere through frictional wear (Gietl et al., 2010; Hulskotte et al., 2014). In 2016, traffic in front of the Castle and

the Enid A. Haupt Gateposts averaged 26,358 cars per weekday (Figure S3), making vehicles a likely source of barite in the Smithsonian Castle’s urban setting.

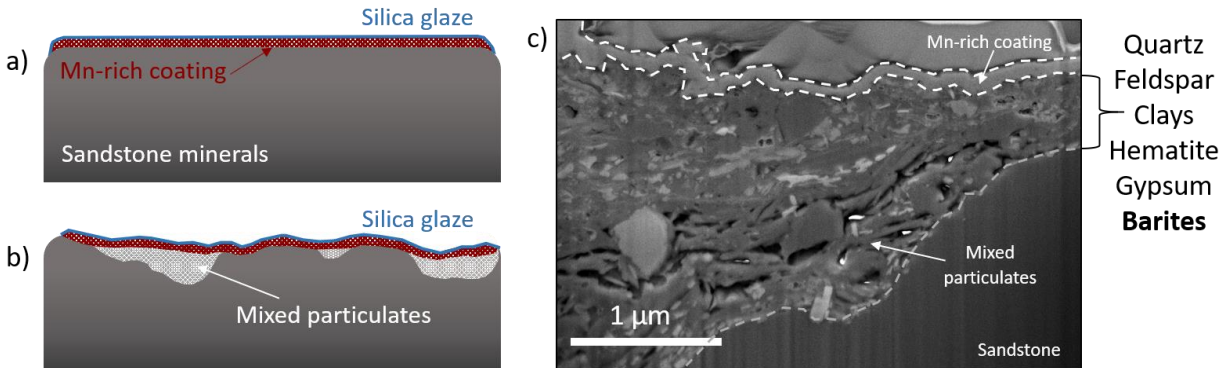


Figure 6: Schematic representations of the two types of stratigraphy seen in the FIB sections. a) A schematic representation of Fig. 3a, where a Mn-film sits on top of a sandstone grain, b) A schematic representation of (c), where the Mn-rich film sits on top of particulates consisting of quartz, feldspar, clays, hematite, gypsum, and barite. In these representations, a thin, silica glaze (only observable by HRTEM) sits on top of the Mn-rich coating. c) SE image of the mixed particulate layer. The brighter particles are Ba-rich.

Atmospheric deposition of barite particles and their location within both detritus and varnish provide a relative timeline of formation for the varnish based on the nano-stratigraphy. The sediment layer below the varnish must have been deposited through aeolian processes first, followed by formation of the Ca-rich birnessite. A thin layer of silica is forming as the most recent stage in deposition, as indicated by the EDX map in Figure 5. In one case, a thin layer of silica resides within the varnish as well as on top of it (Figure S4). Silica glazes form relatively quickly (on decadal timescales) through the mobilization of soluble silicon complexes that spread through surface wetting (Langworthy et al., 2010), or in high humid environments (Dorn, 2013). Silica glazes have been shown to form in many terrestrial environments (Dorn, 1998), including urban areas (McAlister et al., 2006; Smith et al., 2007). Given the humid subtropical climate of Washington, D.C. and the abundance of silicon in the sandstone, it is perhaps unsurprising that a

silica glaze is forming, but it is interesting to note that it is only observable using high resolution imaging.

3.3 Reclassifying the varnish as a manganese skin

The heavy enrichment of Mn in the Castle's discolored surface layer (>1000x over the underlying Seneca sandstone) and the abundance of Mn oxide relative to clay minerals denotes a compositional and mineralogical departure from traditional rock varnish formed in arid settings. Enrichment of Mn oxides similar to what we see here has been reported for varnishes in climates that have high humidity and receive significant rainfall but that vary widely in temperature (Casanova Municchia et al., 2016; Goossens et al., 2015; Krinsley et al., 2017). In one of these studies investigating a varnish in southern Belgium, Goossens et al. (2015) suggest that macroscopically, the black patina is easily misidentified as a varnish, but that chemically it is better described as an Fe/Mn-rich heavy metal skin. Classifications of rock coatings by Dorn (1998) specify that an overwhelming dominance of Mn indicates the formation of a manganese skin, as opposed to rock varnish, which by definition has a layered texture dominated by clay minerals (Dorn et al., 2012a). Manganese skins are typically found in wetter climates and locations, and those rich in birnessite are common in caves (Hill, 1982; White et al., 2009), on rocks and pebbles in streams (Robinson, 1993; Tani et al., 2003), in soils near springs (Mustoe, 1981), and underneath glaciers (Dorn, 1998; Potter and Rossman, 1979). The chemical similarities between these previous studies and the analysis presented here indicate that the dark growth on the Castle is also best described as a manganese skin. The Washington, D. C. climate (a humid, sub-tropical zone) likewise supports this designation.

The classification of the Castle coating as a manganese skin carries some implications for growth rates and biological origins that prompt further discussion. Manganese skins grow much

faster than varnishes, covering surfaces within a single year in certain environments (Dorn, 1998; Dorn and Meek, 1995). Similarly, rock varnishes enriched in Mn have been reported with growth rates faster than the 1-40 $\mu\text{m}/\text{ka}$ observed by Liu and Broecker (2000). Spilde et al. (2013) highlights that ‘active’ and ‘non-active’ periods of growth could account for rate discrepancies throughout the literature, while Dorn and Meek (1995) and Krinsley et al. (2017) suggest that rapid varnish growth could be due to cocci bacteria residing on rock surfaces. Biologically mediated Mn oxides often have sheet structures like birnessite or buserite (Tebo et al., 2004; Villalobos et al., 2003). Krinsley et al. (2012) also make an association between humid environments, faster varnish growth rates, and a greater presence of Mn-enhancing microorganisms. For manganese skins, faster growth rates are attributed to microorganisms that act as oxidation catalysts for Mn^{2+} ; inorganic catalysts (including iron hydroxides) oxidize Mn^{2+} more slowly than bacteria (Diem and Stumm, 1984; Nealson, 2006; Robinson, 1993). Abiotic methods of formation are only viable in certain environments where pH can fluctuate to support the alkaline conditions necessary for physicochemical oxidation, such as where two bodies of water mix (Dorn, 1998).

The presence and location of barite (discussed in section 3.2) in the rock coating and in detritus beneath the coating indicate that the Mn-rich layer may be significantly younger than the age of the Castle, particularly if the source of Ba is related to vehicle brake wear. This Mn-rich film is also present on the Enid A. Haupt Garden gateposts, which were erected just over 30 years ago (Vicenzi et al., 2016), placing it among the timelines of other rapidly forming manganese skins and varnishes, i.e. $>40 \mu\text{m}/\text{ka}$. However, while the literature on manganese skins and rapidly growing varnishes speculates that growth rates are linked to a biological origin, we find no direct microstructural evidence in the form of microorganism casts or casings on the Castle sandstone (Krinsley, 1998), and biological testing is beyond the scope of this study. We did observe bacterial

remains in the form of filaments (Figure S5), but these were rare, found on top of the Mn-rich layer, and were associated with Fe oxide rather than Mn oxide enrichment.

Conclusion

We performed a nanoscale analysis to investigate the composition and structure of the Mn-rich varnish accumulating on the Smithsonian Castle using a combination of electron microscopy and X-ray spectroscopies. SEM/FIB and subsequent TEM analysis revealed that the primary mineralogical phase of the varnish is Ca-rich birnessite, a layered phyllomanganate. The Mn-rich film is <1 μm thick in the areas studied and contains only minor quantities of Fe, Si, and Al. The high levels of Mn, over 1000x the concentration in the underlying Seneca sandstone, and the relative scarcity of clay minerals within the same layer indicate that the ‘varnish’ should instead be classified as a heavy metal skin. Evidence of nanoscale barite, both in the Mn-rich film and within a layer of detritus below the film, suggests atmospheric deposition of BaSO_4 (potentially related to vehicle brake wear), as Ba is found only in trace quantities in the underlying Seneca sandstone. The presence of BaSO_4 throughout the nano-stratigraphy also reveals a relative timeline of film growth and supports a growth rate faster than is typical for rock varnish. The presence of a manganese skin, the fast growth rate, and the wet climate in which the film is forming all suggest that an abiotic hypothesis of origin is unlikely; however, we did not find direct evidence supporting a biogenic origin of formation.

Statement of Interest

The authors declare no competing interests.

Acknowledgements

The research presented here was made possible through the U.S. National Science Foundation’s Graduate Research Internship Program (GRIP). MCS is funded by the NSF Graduate Research

Fellowship Program under Grant No. 1309047 and was partially supported on this project by the University of Oregon (UO) Graduate School through a Special Opportunity Award. The FIB and TEM work were performed with the help of Robert Fischer and Josh Razink at the Center for Advanced Materials Characterization in Oregon (CAMCOR), located at the UO. CAMCOR instruments and facilities were purchased with a combination of federal and state funding. MCS would also like to acknowledge Dr. James Hutchison and Dr. Darren Johnson at UO for their feedback and guidance on the GRIP proposal. EPV is supported as a guest researcher at the National Institute of Standards and Technology (NIST) in Gaithersburg, MD, where μ XRF analysis was performed. This project also received support from the Smithsonian's Museum Conservation Institute, and we acknowledge the assistance of Sharon Park with Smithsonian Institution Facilities.

References

- Allen, C.C. et al., 2004. Meridiani Planum hematite deposit and the search for evidence of life on Mars—iron mineralization of microorganisms in rock varnish. *Icarus*, 171(1): 20-30.
- Anthony, J.W., Bideaux, R.A., Bladh, K.W., Nichols, M.C., eds., 1997. *Handbook of Mineralogy*. Mineralogical Society of America, Chantilly, VA 20151-1110, USA.
- Broecker, W.S., Liu, T., 2001. Rock Varnish: Recorder of Desert Wetness? *GSA Today*, 11(8).
- Casanova Municchia, A. et al., 2016. Characterization of an unusual black patina on the Neang Khmau temple (archaeological Khmer area, Cambodia): a multidisciplinary approach. *Journal of Raman Spectroscopy*, 47(12): 1467-1472.
- Diem, D., Stumm, W., 1984. Is dissolved Mn²⁺ being oxidized by O₂ in absence of Mn-bacteria or surface catalysts? *Geochimica et Cosmochimica Acta*, 48(7): 1571-1573.
- Dorn, R.I., 1998. *Rock Coatings. Developments in earth surface processes*. Elsevier, Amsterdam New York, 429 pp.
- Dorn, R.I., 2007. Rock Varnish. In: Nash, D.J., McLaren, S.J. (Eds.), *Geochemical Sediments and Landscapes*. Blackwell Publishing Ltd., Oxford, UK, pp. 246-297.
- Dorn, R.I., 2013. Formation of Silica Glaze Rock Coatings through Water Vapor Interactions. *Physical Geography*, 33(1): 21-31.
- Dorn, R.I., Krinsley, D., 2011. Spatial, temporal and geographic considerations of the problem of rock varnish diagenesis. *Geomorphology*, 130(1-2): 91-99.
- Dorn, R.I., Krinsley, D.H., Ditto, J., 2012a. Revisiting Alexander von Humboldt's Initiation of Rock Coating Research. *The Journal of Geology*, 120(1): 1-14.
- Dorn, R.I., Krinsley, D.H., Langworthy, K.A., Ditto, J., Thompson, T.J., 2013. The influence of mineral detritus on rock varnish formation. *Aeolian Research*, 10: 61-76.

- Dorn, R.I. et al., 1992. Manganese-rich rock varnish does occur in Antarctica. *Chemical Geology*, 99(4): 289-298.
- Dorn, R.I., Meek, N., 1995. Rapid formation of rock varnish and other rock coatings on slag deposits near Fontana, California. *Earth Surface Processes and Landforms*, 20(6): 547-560.
- Dorn, R.I. et al., 2012b. Assessing Early Spanish Explorer Routes Through Authentication of Rock Inscriptions. *The Professional Geographer*, 64(3): 415-429.
- Drits, V.A., Lanson, B., Gorshkov, A.I., Manceau, A., 1998. Substructure and superstructure of four-layer Ca-exchanged birnessite. *American Mineralogist*, 83(1-2): 97-118.
- Elvidge, C.D., Moore, C.B., 2013. Restoration of petroglyphs with artificial desert varnish. *Studies in Conservation*, 25(3): 108-117.
- Engel, C.G., Sharp, R.P., 1958. Chemical Data on Desert Varnish. *Geological Society of America Bulletin*, 69(5).
- Fleisher, M., Liu, T., Broecker, W.S., Moore, W., 1999. A clue regarding the origin of rock varnish. *Geophysical Research Letters*, 26(1): 103-106.
- Garvie, L.A.J., Burt, D.M., Buseck, P.R., 2008. Nanometer-scale complexity, growth, and diagenesis in desert varnish. *Geology*, 36(3).
- Gietl, J.K., Lawrence, R., Thorpe, A.J., Harrison, R.M., 2010. Identification of brake wear particles and derivation of a quantitative tracer for brake dust at a major road. *Atmospheric Environment*, 44(2): 141-146.
- Goossens, D. et al., 2015. Rock fragments with dark coatings in slope deposits of the Famenne region, southern Belgium. *Belgeo*(4).
- Grissom, C.A., Aloiz, E.M., Vicenzi, E.P., Livingston, R.A., 2018. Seneca sandstone: a heritage stone from the USA. Geological Society, London, Special Publications.
- Grissom, C.A. et al., 2014. Manganese in Black Crusts on Seneca Sandstone. *Microscopy and Microanalysis*, 20(S3): 2044-2045.
- Hill, C.A., 1982. Origin of black deposits in caves. *The National Speleological Society*, 44(1): 15-19.
- Hulskotte, J.H.J., Roskam, G.D., Denier van der Gon, H.A.C., 2014. Elemental composition of current automotive braking materials and derived air emission factors. *Atmospheric Environment*, 99: 436-445.
- Humboldt, A.v., Wilson, J., 1995. Personal narrative. Penguin classics. Penguin Books, London; New York, 310 pp.
- Krinsley, D., 1998. Models of rock varnish formation constrained by high resolution transmission electron microscopy. *Sedimentology*, 45(4): 711-725.
- Krinsley, D., Dorn, R.I., DiGregorio, B., 2009. Astrobiological implications of rock varnish in Tibet. *Astrobiology*, 9(6): 551-62.
- Krinsley, D.H., DiGregorio, B., Dorn, R.I., Razink, J., Fisher, R., 2017. Mn-Fe-Enhancing Budding Bacteria in Century-Old Rock Varnish, Erie Barge Canal, New York. *The Journal of Geology*, 125(3): 317-336.
- Krinsley, D.H., Dorn, R.I., DiGregorio, B.E., Langworthy, K.A., Ditto, J., 2012. Rock varnish in New York: An accelerated snapshot of accretionary processes. *Geomorphology*, 138(1): 339-351.
- Langworthy, K.A., Krinsley, D.H., Dorn, R.I., 2010. High resolution transmission electron microscopy evaluation of silica glaze reveals new textures. *Earth Surface Processes and Landforms*, 35(13): 1615-1620.

- Lanson, B., Drits, V.A., Feng, Q., Manceau, A., 2002. Structure of synthetic Na-birnessite: Evidence for a triclinic one-layer unit cell. *American Mineralogist*, 87(11-12): 1662-1671.
- Liu, T., Broecker, W.S., 2000. How fast does rock varnish grow? *Geology*, 28(2): 183-186.
- Liu, T., Broecker, W.S., 2007. Holocene rock varnish microstratigraphy and its chronometric application in the drylands of western USA. *Geomorphology*, 84(1-2): 1-21.
- Liu, T., Broecker, W.S., 2008. Rock varnish microlamination dating of late Quaternary geomorphic features in the drylands of western USA. *Geomorphology*, 93(3-4): 501-523.
- Livingston, R.A. et al., 2016. Investigation of Urban Rock Varnish on the Sandstone of the Smithsonian Castle. In: Hughes, J., Howind, T. (Editors), 13th International Congress on the Deterioration and Conservation of Stone, Paisley, Scotland, pp. 399-406.
- Lu, Y., Tang, C.-F., Wright, M.A., 2002. Optimization of a commercial brake pad formulation. *Journal of Applied Polymer Science*, 84(13): 2498-2504.
- Macholdt, D.S., Al-Amri, A.M., Tuffaha, H.T., Jochum, K.P., Andrae, M.O., 2018. Growth of desert varnish on petroglyphs from Jubbah and Shuwaymis, Ha'il region, Saudi Arabia. *The Holocene*, 28(9): 1495-1511.
- Macholdt, D.S. et al., 2017a. Black manganese-rich crusts on a Gothic cathedral. *Atmospheric Environment*, 171: 205-220.
- Macholdt, D.S., Jochum, K.P., Al-Amri, A., Andrae, M.O., 2019. Rock varnish on petroglyphs from the Hima region, southwestern Saudi Arabia: Chemical composition, growth rates, and tentative ages. *The Holocene*, 0(0): 0959683619846979.
- Macholdt, D.S. et al., 2017b. Characterization and differentiation of rock varnish types from different environments by microanalytical techniques. *Chemical Geology*, 459: 91-118.
- McAlister, J.J., Smith, B.J., Török, A., 2006. Element partitioning and potential mobility within surface dusts on buildings in a polluted urban environment, Budapest. *Atmospheric Environment*, 40(35): 6780-6790.
- McKeown, D.A., Post, J.E., 2001. Characterization of manganese oxide mineralogy in rock varnish and dendrites using X-ray absorption spectroscopy. *American Mineralogist*, 86(5-6): 701-713.
- Mustoe, G.E., 1981. Bacterial oxidation of manganese and iron in a modern cold spring. *Geological Society of America Bulletin*, 92: 147-153.
- Nealson, K.H., 2006. The Manganese-Oxidizing Bacteria. In: Dworkin, M., Falkow, S., Rosenberg, E., Schleifer, K.-H., Stackebrandt, E. (Eds.), *The Prokaryotes*. Springer New York, New York, NY, pp. 222-231.
- Northup, D.E. et al., 2010. Diversity of rock varnish bacterial communities from Black Canyon, New Mexico. *Journal of Geophysical Research: Biogeosciences*, 115(G2): n/a-n/a.
- Ortiz-Montalvo, D.L. et al., 2018. Chemical Compound Classification by Elemental Signatures in Castle Dust Using SEM Automated X-ray Particle Analysis. *Microscopy and Microanalysis*, 24(S1): 718-719.
- Peck, G., 2013. *The Smithsonian Castle and the Seneca Quarry*. The History Press, Charleston, SC, 162 pp.
- Perry, R.S., Adams, J.B., 1978. Desert Varnish: Evidence for Cyclic Deposition of Manganese. *Nature*, 276.
- Post, J.E., 1999. Manganese oxide minerals: crystal structures and economic and environmental significance. *Proc Natl Acad Sci U S A*, 96(7): 3447-54.
- Potter, R.M., Rossman, G.R., 1977. Desert varnish: the importance of clay minerals. *Science*, 196(4297): 1446-8.

- Potter, R.M., Rossman, G.R., 1979. Mineralogy of manganese dendrites and coatings. *American Mineralogist*, 64: 1219-1226.
- Raymond, R., Guthrie, G.D., Bish, D.L., Reneau, S.L., 1992. Biomineralization of manganese within rock varnish. *Catena Supplement*(21): 321-335.
- Reneau, S.L., Raymond, R., Harrington, C.D., 1992. Elemental Relationships in Rock Varnish Stratigraphic Layers, Cima Volcanic Field, California: Implications for Varnish Development and the Interpretation of Varnish Chemistry. *American Journal of Science*, 292: 684-723.
- Ritchie, N.W., 2009. Spectrum simulation in DTSA-II. *Microsc Microanal*, 15(5): 454-68.
- Robinson, G.D., 1993. Major-Element Chemistry and Micromorphology of Mn-Oxide Coatings on Stream Alluvium. *Applied Geochemistry*, 8(6): 633-642.
- Smith, B.J., McAlister, J.J., Baptista Neto, J.A., Silva, M.A.M., 2007. Post-depositional modification of atmospheric dust on a granite building in central Rio de Janeiro: implications for surface induration and subsequent stone decay. *Geological Society, London, Special Publications*, 271(1): 153-166.
- Spilde, M.N., Melim, L.A., Northup, D.E., Boston, P.J., 2013. Anthropogenic lead as a tracer of rock varnish growth: Implications for rates of formation. *Geology*, 41(2): 263-266.
- Tani, Y. et al., 2003. Biogeochemistry of manganese oxide coatings on pebble surfaces in the Kikukawa River System, Shizuoka, Japan. *Applied Geochemistry*, 18(10): 1541-1554.
- Tebo, B.M. et al., 2004. BIOGENIC MANGANESE OXIDES: Properties and Mechanisms of Formation. *Annual Review of Earth and Planetary Sciences*, 32(1): 287-328.
- Thiagarajan, N., Aeolus Lee, C.-T., 2004. Trace-element evidence for the origin of desert varnish by direct aqueous atmospheric deposition. *Earth and Planetary Science Letters*, 224(1-2): 131-141.
- Vicenzi, E.P., Grissom, C.A., Livingston, R.A., Weldon-Yochim, Z., 2016. Rock varnish on architectural stone: microscopy and analysis of nanoscale manganese oxide deposits on the Smithsonian Castle, Washington, DC. *Heritage Science*, 4(1).
- Villalobos, M., Bargar, J., Sposito, G., 2005. Trace Metal Retention on Biogenic Manganese Oxide Nanoparticles. *Elements*, 1(4): 223-226.
- Villalobos, M., Toner, B., Bargar, J., Sposito, G., 2003. Characterization of the manganese oxide produced by *pseudomonas putida* strain MnB1. *Geochimica et Cosmochimica Acta*, 67(14): 2649-2662.
- Wang, Y., Feng, X., Villalobos, M., Tan, W., Liu, F., 2012. Sorption behavior of heavy metals on birnessite: Relationship with its Mn average oxidation state and implications for types of sorption sites. *Chemical Geology*, 292-293: 25-34.
- White, W.B., Vito, C., Scheetz, B.E., 2009. The Mineralogy and Trace Element Chemistry of Black Manganese Oxide Deposits from Caves. *Journal of Cave and Karst Studies*, 71(2): 136-143.